$BaCu_{10}P_4$: A New Structure Composed of Chains of Edge-Shared Cu_4 Tetrahedra

Dianna M. Young, John Charlton, Marilyn M. Olmstead, and Susan M. Kauzlarich*

Department of Chemistry, University of California, Davis, California 95616

Chi-Shen Lee and Gordon J. Miller*

Department of Chemistry, Iowa State University, Ames, Iowa 50011

Received November 6, 1996[⊗]

A new barium copper phosphide compound, $BaCu_{10}P_4$, was synthesized by reacting stoichiometric amounts of the elements at 1200 °C for 24 h. $BaCu_{10}P_4$ crystallizes in the monoclinic space group *C2/m*, with unit cell dimensions $a = 23.288(4)$ $b = 3.9070(10)$, and $c = 9.534(2)$ Å and $\beta = 92.26(2)°$ ($Z = 4$). The structure can be described as consisting of chains of edge-shared Cu_4 tetrahedral prisms that are knitted together by P atoms. The structure is related to $BaCu_8P_4$, which can be described in a similar fashion. Temperature-dependent resistivity measurements indicate that $BaCu_{10}P_4$ is a metal. Extended Hückel band calculations are consistent with metallic character for $BaCu_{10}P_4$ through Cu−Cu interactions. Orbitals at the Fermi level show Cu−Cu bonding overlap. On the other hand, $BaCu_8P_4$ reveals extremely weak Cu−Cu interactions, but rather optimizes Cu−P bonding.

Introduction

Ternary transition metal phosphides display a variety of structures and properties. In particular, ternary metal-rich lanthanoid (Ln) transition metal (M) phosphides such as $Ln_2M_{12}P_7$[1] have been well studied. These structures feature phosphorus atoms with characteristic trigonal prismatic metal coordination.[2] Metal-rich alkaline earth transition metal phosphides form a smaller, less well-characterized group of compounds. Although a few crystallize in the structure types afforded the lanthanoid transition metal phosphides, many do not appear to be structurally related. To date, there are only six examples of structurally characterized ternary barium copper phosphorus compounds. The compounds, BaCuP,[3] $BaCu_2P_4$,[4] $Ba_2Cu_3P_4$,[5] $BaCu_6P_2$,[6] $Ba_8Cu_{16}P_{30}$,[7] and $BaCu_8P_4$,[8] investigated by Mewis and co-workers, have been classified as either intermetallic or Zintl compounds. BaCuP and $Ba_2Cu_3P_4$ are layered structures and crystallize in a modified Ni_2In and $ThCr_2Si_2$ structure type, respectively. $BaCu_6P_2$ is described as an intergrowth of $ThCr_2Si_2$ and Cu structure types. $BaCu_2P_4$, $Ba_8Cu_{16}P_{30}$, and $BaCu_8P_4$ show structural similarities such as three-dimensionally linked CuP_4 tetrahedra that form large, open cavities in which the Ba atoms reside. The CuP_4 tetrahedra in $BaCu_2P_4$ are edge-shared, and the Cu and P atoms are stacked along the *a* axis, giving rise to parallel helical chains of phosphorus atoms reminiscent of $^1_\infty[P^-]$ found in the Zintl compound CdP_2. The CuP_4 tetrahedra in $BaCu_8P_4$ are linked to form a three-dimensional framework, providing two different channels along the *c* axis in which Ba atoms and chains of edge-shared Cu_4 tetrahedra are located.

While investigating the synthesis and properties of $BaCu_8P_4$, we discovered a new compound, $BaCu_{10}P_4$. It is a new structure type that resembles $BaCu_8P_4$ and can be considered the reduced form of that compound. All the Cu atoms in $BaCu_{10}P_4$ must be formally Cu^I, whereas in $BaCu_8P_4$ they must consist of six Cu^I and two Cu^{II} atoms. An alternate view of the bonding in $BaCu_8P_4$ recognizes the Cu_4 units as four-center-two-electron clusters, formally $(Cu_4)^{6+}$, and the remaining four Cu atoms are considered Cu^I to balance the charge of $4P^{3-}$ and Ba^{2+}. The category of borderline Zintl phases consist of compounds with "locally delocalized electrons", that do not conform to the octet rule, and mark the transition to intermetallic phases.[9] The chemical bonding in borderline Zintl phases is not well understood, and the phases are rich in structural chemistry; thus, investigating these borderline phases promises new information about structure−property relationships of inorganic compounds. The few barium copper phosphide compounds that have been investigated suggest that they can be considered borderline Zintl phases. The synthesis, structure, and electronic properties of $BaCu_{10}P_4$ will be presented and compared with those of $BaCu_8P_4$ and other known copper phosphide compounds.

Experimental Section

Synthesis. Crystals of $BaCu_{10}P_4$ were initially obtained in low yield by reacting the elements Ba (99.99%, J. Matthey), Cu (99.99%, Aesar), and P (99.99% Strem) in the ratio 1:8:4 (Ba:Cu:P). Cu and P were mixed together in the form of powder, with Ba cut into small pieces, and pressed into a pellet in a nitrogen-filled drybox. The pellet was put into an alumina boat that was then sealed in a quartz tube under vacuum. The reaction was heated at 60 °C/h to 950 °C, maintained at that temperature for 24 h, and subsequently cooled at 60 °C/h to room temperature. The resulting non-air-sensitive product was typically made up of highly reflective silver/black chunks of material, powder, and a small amount of long, black needle crystals. Guinier powder X-ray diffraction indicated that the majority of the product was the $BaCu_8P_4$, and single-crystal X-ray diffraction indicated that the rectangular needles were $BaCu_{10}P_4$. Reactions to produce $BaCu_{10}P_4$ were set up with the ratio of 1:10:4 (Ba:Cu:P), rapidly heated to 800 °C, heated at 60 °C/h to 1200 °C, maintained at 1200 °C for 24 h, and subsequently cooled at 60 °C/h to 800 °C. Guinier powder diffraction indicated that $BaCu_{10}P_4$ is obtained in quantitative yield.

[⊗] Abstract published in *Advance ACS Abstracts,* May 1, 1997.

(1) Villars, P.; Calvert, L. *Pearson's Handbook of Crystallographic Data for Intermetallic Phases,* 2nd ed.; American Society for Metals: Materials Park, OH, 1991.
(2) Pivan, J.-Y.; Guérin, R.; Sergent, M. *J. Solid State Chem.* **1987**, *68*, 11.
(3) Mewis, A. *Z. Naturforsch., B* **1979**, *34*, 1373.
(4) Dünner, J.; Mewis, A. *J. Less-Comm. Metals* **1990**, *167*, 127.
(5) Pilchowski, I.; Mewis, A. *Z. Anorg. Allg. Chem.* **1990**, *581*, 173.
(6) Dünner, J.; Mewis, A. *J. Alloys Compd.* **1995**, *221*, 65.
(7) Dünner, J.; Mewis, A. *Z. Anorg. Allg. Chem.* **1995**, *621*, 191.
(8) Pilchowski, I.; Mewis, A.; Wenzel, M.; Gruehn, R. *Z. Anorg. Allg. Chem.* **1990**, *588*, 109.
(9) Nesper, R. *Angew. Chem., Int. Ed. Engl.* **1991**, *30*, 789.

S0020-1669(96)01347-X CCC: $14.00

Table 1. Selected Data Collection and Refinement Parameters for $BaCu_{10}P_4$[a]

chemical formula	$BaCu_{10}P_4$	formula weight	896.62
a (Å)	23.288(4)	space group	$C2/m$
b (Å)	3.9070(10)	T (°C)	−143
c (Å)	9.534(2)	λ (Mo Kα, Å)	0.710 69
β (deg)	92.26(2)	ρ_{calc} (g cm^{-3})	6.871
V (Å^3)	866.8(3)	μ cm^{-1}	291.1
Z	4	$R1$ [$I > 2\sigma(I)$][b]	4.68%
		$wR2$ [$I > 2\sigma(I)$][b]	13.48%

[a] Room temperature lattice parameters are a = 23.338(7), b = 3.918(1), and c = 9.529(2) Å and β = 92.26(1)°. [b] $R(F) = ||F_o| - |F_c||/\sum|F_o|$ and $R_w(F_o^2) = [(w(F_o^2 - F_c^2)^2/\sum wF_o^4)]^{1/2}$; $w^{-1} = 1/[\sigma^2(F_o^2) + (0.1090p)^2 + 7.97p]$, where $p = (\max(F_o^2,0) + 2F_c^2)/3$.

Attempts were made to grow large crystals of $BaCu_{10}P_4$ by means of a Sn flux. $BaCu_{10}P_4$ was ground into a powder and mixed with Sn in a 1:10 ratio ($BaCu_{10}P_4$:Sn). The mixture was sealed in quartz under vacuum and heated to 800 °C for 1 week. The products were washed with dilute HCl. Large crystals of $BaCu_8P_4$ were obtained. There was no evidence for $BaCu_{10}P_4$ in the powder diffraction pattern.

Powder X-ray Diffraction. The diffraction pattern of $BaCu_{10}P_4$ was obtained with an Enraf Nonius Guinier powder camera (monochromatic Cu Kα_1 radiation) at room temperature; lattice parameters are given in Table 1. Typical procedures for obtaining powder diffraction data have been described in detail previously.[10] Tables of calculated versus experimental d spacings and intensities are provided as supplemental material.

Single-Crystal X-ray Diffraction. A needle-shaped, black crystal of dimensions 0.43 mm × 0.30 mm × 0.02 mm was used for single-crystal X-ray diffraction measurements. The crystal selected for data collection was mounted on a glass fiber and positioned on a diffractometer equipped with a cold stream of nitrogen. Data were collected ($2\theta_{max} = 65°$, $-34 \le h \le 34$, $0 \le k \le 5$, $0 \le l \le 14$) on a Siemens R3m diffractometer (Mo Kα wavelength = 0.710 69 Å) at 130 K. The unit cell dimensions and crystal system were determined by least-squares refinement of 14 reflections ($16° < 2\theta < 21°$) using the automatic indexing routine of the P3 diffractometer software. Axial photos were taken at long exposure (20 min) to confirm cell dimensions and to check for possible superstructure. No decomposition of the crystal was observed during the data collection, based on the intensity of two check reflections monitored every 198 reflections. In all, 1800 reflections were collected (1776 independent; 1639 observed [$F_o > 4\sigma(F_o)$]. The data were corrected for Lorentz and polarization effects. The crystallographic parameters are summarized in Table 1.

The $BaCu_{10}P_4$ structure was solved and refined with SHELXTL-PLUS[11] programs, and the final refinements and absorption correction were performed in SHELXL-93.[12] Scattering factors and dispersion values are from the *International Tables for Crystallography*.[13] The choice of $C2/m$ was supported by subsequent calculations. The atoms were assigned to relevant intensity peaks and refined with isotropic U values. After convergence, an empirical absorption correction XABS2,[14] was applied. Table 2 lists atomic coordinates and isotropic U values. Tables of complete crystallographic parameters and anisotropic displacement parameters are provided in the Supporting Information.

Resistivity. Data were obtained both on polycrystalline pieces and on a single crystal. A polycrystalline piece was isolated and placed on a small piece of alumina in which four 0.002 in. diameter platinum leads were attached. The leads were mounted on the piece with silver epoxy. The epoxy was then cured by transferring the sample to a furnace and heating to 100 °C for 1 h under vacuum. Leads were attached in a similar fashion to a single crystal of approximate dimensions 1.1 mm × 0.4 mm × 0.4 mm. The sample was mounted on a closed cycle refrigerator and the sample chamber evacuated. The temperature-dependent dc resistivity was measured using the four-probe technique, and samples were measured from 15 to 300 K, in 5 K increments. The resistivity apparatus has been described in detail previously,[10] and data were collected with the program DCRES.[15] Minimization of thermal voltages was achieved by reversal of current bias. All samples exhibited ohmic behavior.

Table 2. Atomic Coordinates ($\times 10^4$) and Equivalent Isotropic Displacement Parameters (Å^2 × 10^3) for $BaCu_{10}P_4$

atom	x	y	z	U_{eq}[a]
Ba(1)	3567(1)	5000	2173(1)	5(1)
Cu(1)	2768(1)	0	4311(1)	6(1)
Cu(2)	4666(1)	0	3817(1)	8(1)
Cu(3)	4741(1)	0	1182(1)	6(1)
Cu(4)	5490(1)	5000	720(1)	7(1)
Cu(5)	2878(1)	0	6973(1)	8(1)
Cu(6)	3331(1)	5000	5729(1)	7(1)
Cu(7)	3491(1)	5000	8529(1)	8(1)
Cu(8)	2862(1)	0	−354(1)	8(1)
Cu(9)	4427(1)	5000	5468(1)	10(1)
Cu(10)	4145(1)	0	7274(2)	16(1)
P(1)	4920(1)	5000	2662(2)	7(1)
P(2)	3773(1)	0	4986(2)	5(1)
P(3)	2467(1)	0	1912(2)	4(1)
P(4)	3926(1)	0	−363(2)	5(1)

[a] U_{eq} is defined as one-third of the trace of the orthogonalized $\mathbf{U_{ij}}$ tensor.

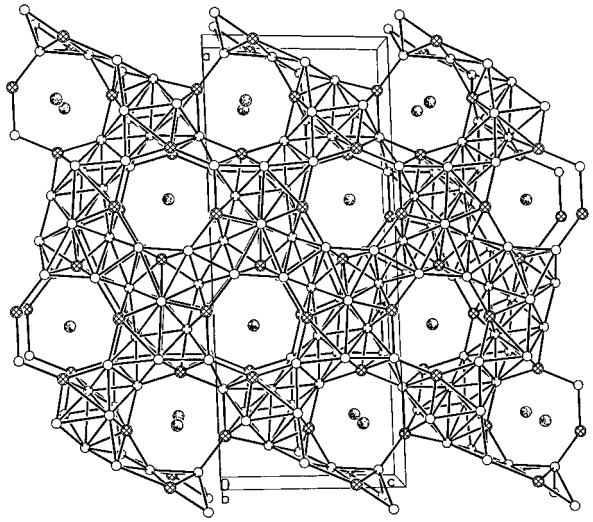

Figure 1. Perspective view down the b axis of $BaCu_{10}P_4$. Ba, Cu, and P atoms are indicated by dotted, open, and cross-hatched circles, respectively.

Electronic Structure Calculations. All electronic structure calculations used the extended Hückel method within the framework of the tight-binding approximation.[16−19] Two nearest-neighbor shells were included. Atomic parameters for the elements are listed in Table 4. Atomic populations and overlap populations were determined using a special points set (eight points for monoclinic $BaCu_{10}P_4$; 30 points for $BaCu_8P_4$).[20]

Results and Discussion

Figure 1 shows a perspective view of $BaCu_{10}P_4$ down the b axis. Selected bond distances are listed in Table 3. The $BaCu_{10}P_4$ structure is a complicated three-dimensional network

(10) Young, D. M.; Torardi, C. C.; Olmstead, M. M.; Kauzlarich, S. M. *Chem. Mater.* **1995**, *7*, 93.
(11) Sheldrick, G. M. SHELXTL-PLUS, Version 4.21, Madison, WI, 1990.
(12) Sheldrick, G. M. *J. Appl. Crystallogr.* In preparation.
(13) *International Tables for Crystallography*; Reidel Publishing Co.: Boston, 1992; Vol. C.
(14) Parkin, S.; Moezzi, B.; Hope, H. *J. Appl. Crystallogr.* **1995**, *28*, 53.
(15) Sunstrom, J. E., IV. DCRES: A Quickbasic program for temperature dependent resistivity data collection and analysis, University of California, Davis, 1991.
(16) Hoffmann, R.; Lipscomb, W. N. *J. Chem. Phys.* **1962**, *36*, 2179.
(17) Hoffmann, R. *J. Chem. Phys.* **1963**, *39*, 1397.
(18) Ammeter, J. H.; Bürgi, H.-B.; Thibeault, J. C.; Hoffmann, R. *J. Am. Chem. Soc.* **1978**, *100*, 3686.
(19) Whangbo, M.-H.; Hoffmann, R.; Woodward, R. B. *Proc. R. Soc. London* **1979**, *A366*, 23.
(20) Chadi, D. J.; Cohen, M. L. *Phys. Rev. B* **1973**, *8*, 5747.

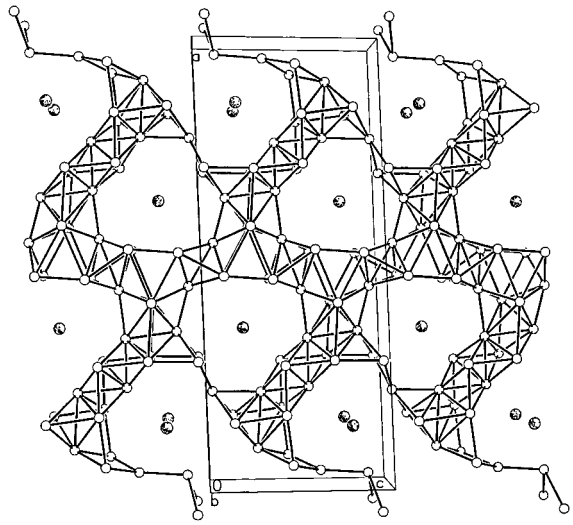

Figure 2. Perspective view down the *b* axis of $BaCu_{10}P_4$ in which the P atoms have been removed. Ba and Cu atoms are indicated by dotted and open circles, respectively.

Table 3. Selected Bond Distances (Å) for $BaCu_{10}P_4$

Cu(1)−P(3)	2.366(2)	Cu(5)−P(3) (×2)	2.379(1)
Cu(1)−P(2)	2.402(2)	Cu(5)−Cu(6) (×2)	2.537(1)
Cu(1)−Cu(5)	2.541(2)	Cu(5)−Cu(8)	2.550(2)
Cu(1)−Cu(6) (×2)	2.559(2)	Cu(5)−Cu(7) (×2)	2.809(1)
Cu(1)−Cu(6) (×2)	2.687(1)	Cu(5)−P(2)	2.871(2)
Cu(1)−Cu(1) (×2)	2.689(1)	Cu(5)−Cu(10)	2.955(2)
Cu(1)−Cu(5) (×2)	2.726(1)		
Cu(1)−Ba(1)	3.465(1)	Cu(6)−P(2) (×2)	2.331(1)
		Cu(6)−Cu(5) (×2)	2.537(1)
Cu(2)−P(1) (×2)	2.330(1)	Cu(6)−Cu(9)	2.574(2)
Cu(2)−P(2)	2.398(3)	Cu(6)−Cu(7)	2.680(2)
Cu(2)−Cu(3)	2.526(2)	Cu(6)−Cu(10)	3.060(2)
Cu(2)−Cu(9) (×2)	2.583(1)		
Cu(2)−Cu(2)	2.689(2)	Cu(7)−P(3)	2.255(2)
Cu(2)−Cu(9) (×2)	2.937(1)	Cu(7)−P(4) (×2)	2.424(2)
Cu(2)−Cu(10)	2.996(2)	Cu(7)−Cu(8) (×2)	2.688(1)
Cu(2)−Ba(1)	3.536(1)	Cu(7)−Cu(10) (×2)	2.777(1)
		Cu(7)−Cu(5)	2.809(1)
Cu(3)−P(4)	2.355(2)	Cu(7)−Ba(1)	3.473(1)
Cu(3)−P(1) (×2)	2.436(2)		
Cu(3)−Cu(3)	2.598(2)	Cu(8)−P(3)	2.380(2)
Cu(3)−Cu(4) (×2)	2.668(1)	Cu(8)−P(4)	2.479(2)
Cu(3)−Cu(4) (×2)	2.705(1)	Cu(8)−P(3) (×2)	2.553(2)
Cu(3)−Cu(10)	2.932(1)	Cu(8)−Cu(8) (×2)	2.683(2)
Cu(3)−Ba(1)	3.520(1)	Cu(8)−Ba(1)	3.691(2)
Cu(4)−P(1)	2.321(3)	Cu(9)−P(1)	2.297(3)
Cu(4)−P(4)	2.412(1)	Cu(9)−P(2) (×2)	2.509(2)
Cu(4)−Cu(7)	2.450(2)	Cu(9)−Cu(10) (×2)	2.702(1)
Cu(4)−Cu(4)	2.618(2)	Cu(9)−Cu(9)	2.847(2)
Cu(4)−Cu(3)	2.668(1)		
Cu(4)−Cu(3) (×2)	2.705(1)	Cu(10)−P(2)	2.316(3)
Cu(4)−Cu(10)	2.840(1)	Cu(10)−P(4)	2.330(2)

that shows extensive Cu−Cu bonding. There are large, approximately heptagonal, holes in the Cu−P framework in which the Ba atoms reside. This structure can be simplified by considering the structure to be composed of alternating edge-shared Cu_4 tetrahedra that form chains running along the *b* axis. Figure 2 shows a perspective view with the P atoms omitted which illustrates the Cu−Cu bonding motifs. Figure 3 identifies four distinct Cu_4 edge-shared clusters, **I**, **II**, **III**, and **IV**, and two other unique bonding motifs, **V**, and **VI**, in $BaCu_{10}P_4$. Figure 4 provides a view rotated by 180° which includes the atom labels. The cavity that contains the Ba atom is formed by a seven-membered ring that is closed by a Cu−Cu bond of 2.526(2) Å between Cu(2) (cluster **I**) and Cu(3) (cluster **II**). The Cu−P bond distances within the ring are 2.366(2)−2.526(2)

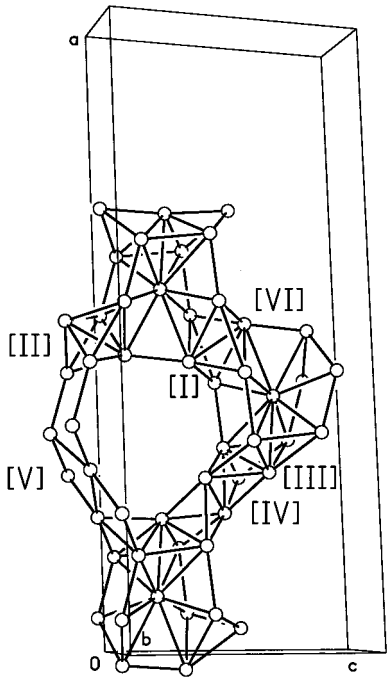

Figure 3. Perspective view of the Cu−Cu bonding showing six motifs of bonding of the Cu atoms, labeled **I**−**VI**.

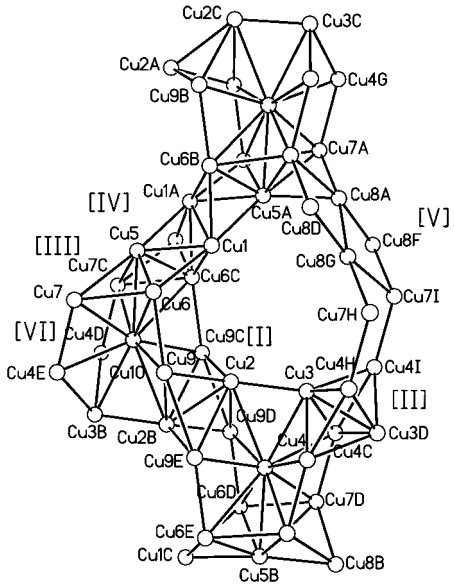

Figure 4. View of the Cu−Cu bonding providing the atoms labels.

Å. **I** and **II** alternate with each other in a linear fashion along the *c* axis and connect the cavities. In addition, **III** is joined to **I** and **II** by means of a Cu atom (Cu(10)), whose coordination is indicated by **VI**. **IV** is edge-shared with **III**, and **V** connects the cavities along *a*.

Figure 5 depicts the four edge-shared sets of tetradrahedra with atoms labels. It is clear from this figure that these units represent two edge-shared tetrahedral prisms of Cu_4. Thus, **I** is made up of two edge-shared tetrahedral prisms of Cu(9,9A,-9B,9C,2,2A) and the shared edge is Cu(2)−Cu(2A), 2.689 (2) Å. The distinctively long distances between Cu(9C) and Cu-(9), Cu(9A), and Cu(9B) atoms of 3.907(1) Å preclude any strong bonding interaction. Other Cu−Cu bond distances in the cluster range from 2.689(2) to 2.937(1) Å. The longer bond distances are similar to those observed in Cu_6 polyhedra of organometallic complexes (2.70−3.06 Å).[21] However, the shorter Cu−Cu distances are comparable to that observed in bulk metal (2.56 Å). **II** has bond distances in the range 2.598-

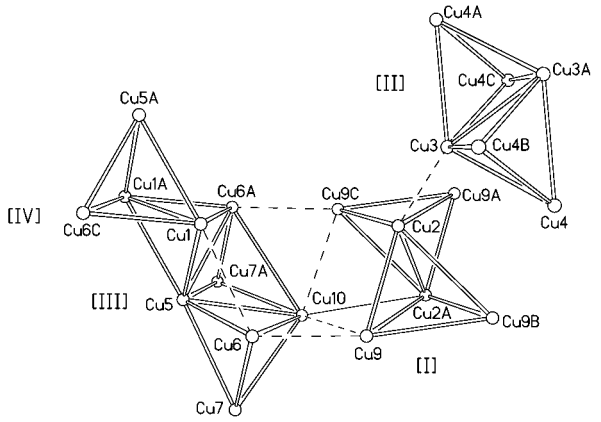

Figure 5. View of the four different edge-shared tetrahedral Cu_4 chains. Dotted lines show how the units are bonding with respect to each other.

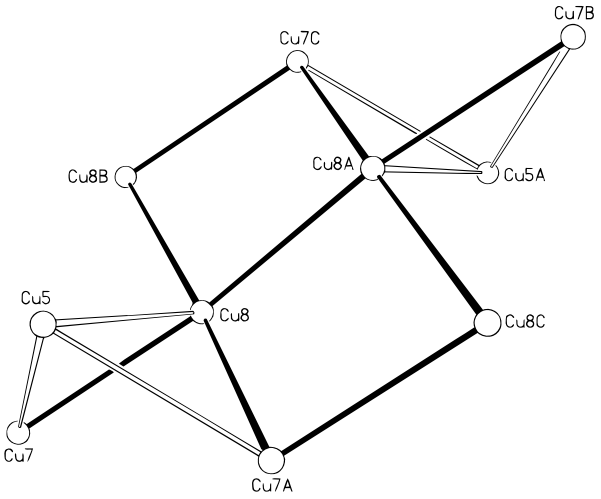

Figure 6. View showing the square planar arrangement of Cu(8) atoms in motif **V**.

(2)−2.705(1) Å and is also bonded to **I** with a short bond of 2.523(1) Å for Cu(3)−Cu(2). **III** consists of Cu(1), Cu(5), and Cu(6) and has bond distances in the range 2.541(2)−2.726(1) Å. Figure 6 shows the square planar arrangement around Cu(8), motif **V**. All the distances are rather short, in the range 2.550(2)−2.688(1) Å. Motif **VI** is best illustrated in Figure 4 and shows Cu(10) as an 11-coordinate capped dodecahedron. Distances from Cu(10) are rather long, ranging from 2.702(1) to 3.060(2) Å.

$BaCu_8P_4$ has been illustrated to emphasize the Cu_4 edge-shared chains.[8] Figure 7 shows a perspective view down the *c* axis of $BaCu_8P_4$, which shows the edge-shared Cu_4 tetrahedral prisms as isolated chains. The deletion of bonds simply allows for a visual simplification of the structure, since the Cu−Cu bond distances between the Cu−P framework are on the same order of magnitude as those within the Cu_4 tetrahedra. The honeycomb-like framework of $BaCu_8P_4$ is simpler than that of $BaCu_{10}P_4$. There are two types of eight-membered rings that form channels, and the rings are composed of alternating Cu and P atoms. The larger channel contains the Ba atoms, and the smaller one contains the chains of edge-shared Cu_4 tetrahedra which run along the *b* axis. The major distinctions between the two structures are the added edge-shared chains in $BaCu_{10}P_4$ and the additional structural motifs of Cu(8) and Cu(10). In addition, the Cu_4 tetrahedral prism in $BaCu_8P_4$ is much more symmetrical than those found in $BaCu_{10}P_4$. The distances of

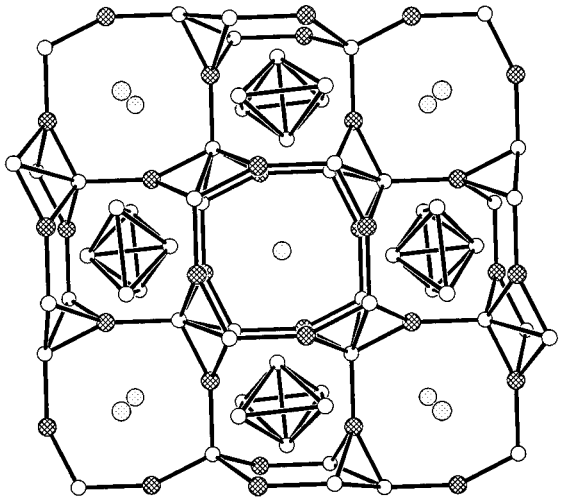

Figure 7. Perspective view down the *c* axis of $BaCu_8P_4$. Ba, Cu, and P atoms are indicated by dotted, open, and cross-hatched circles, respectively.

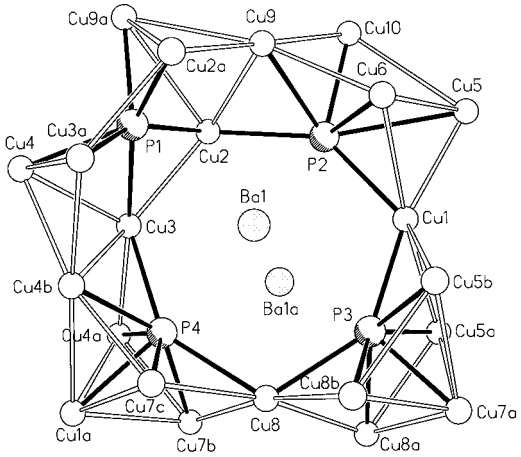

Figure 8. View with atom labels, showing the P coordination sphere in $BaCu_{10}P_4$.

2.754(2) and 2.767(2) Å observed in the Cu_4 unit in $BaCu_8P_4$ are similar to the average distances found in the Cu_4 units in $BaCu_{10}P_4$.

In contrast to metal-rich rare earth phosphides, which typically show trigonal antiprismatic coordination around the P, the P atoms in $BaCu_{10}P_4$ have a variety of coordination geometries. If one includes the Ba atom in the coordination sphere, P(1) is best described as a capped trigonal prism, and P(3) and P(4) are best described as tricapped trigonal prisms. P(2) is 10 coordinate and can be described as a bicapped cuboid coordination. If only the short Cu−P distances are considered in the coordination sphere, P(1) is six coordinate, P(2) is five coordinate, and P(3) and P(4) are seven coordinate. A view illustrating the coordination of P is shown in Figure 8.

The only other electronically characterized barium copper phosphide compound, $BaCu_2P_4$, is also metallic, and its room temperature pressed powder resistivity is reported to be 3.3×10^{-4} Ω cm.[4] The low resistivity observed for $BaCu_2P_4$ has been attributed to the helical chains of phosphorus that run through the structure since there are no Cu−Cu distances less than 2.9 Å. Figure 9 shows temperature-dependent resistivity measurements of a polycrystalline piece of $BaCu_{10}P_4$. Data obtained from the polycrystalline piece and the single crystal were reproducible in their temperature dependence, with the polycrystalline piece showing slightly higher resistivity values. Temperature-dependent resistivity measurements show that $BaCu_{10}P_4$ is metallic and has a room temperature resistivity of

(21) Sabin, F.; Ryu, C. K.; Ford, P. C.; Vogler, A. *Inorg. Chem.* **1992**, *31*, 1941.

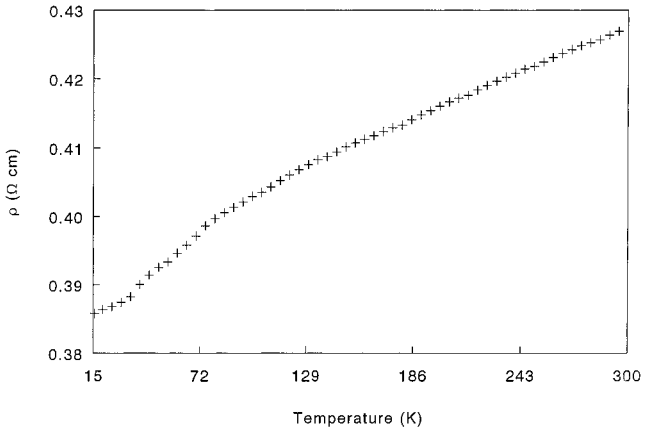

Figure 9. Resistivity versus temperature for $BaCu_{10}P_4$.

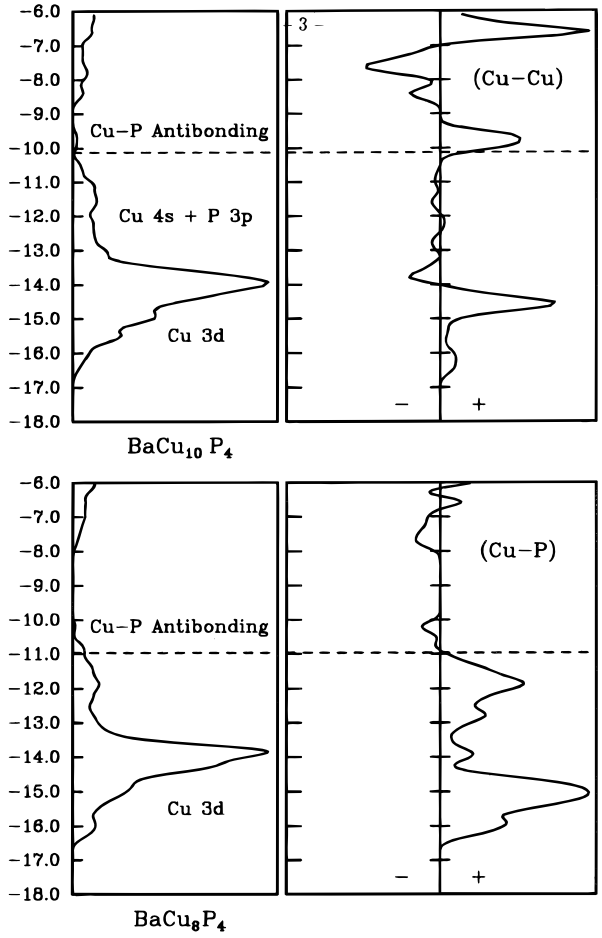

Figure 10. (Top) Total DOS and Cu−Cu COOP curve for $BaCu_{10}P_4$. (Bottom) Total DOS and Cu−P COOP curve for $BaCu_8P_4$. Corresponding Fermi levels are marked by the dashed lines.

$4.3(1) \times 10^{-1}$ Ω cm. The formula suggests that all the Cu is present as Cu^I, and it is expected that the metallic conductivity is a result of the close Cu−Cu distances, which are on the order of those in Cu metal.

This conclusion is supported by extended Hückel calculations. Figure 10 (top) illustrates the total density of states (DOS) for $BaCu_{10}P_4$. The Fermi level occurs near a nonzero minimum in the DOS, which suggests the compound to be a poor metal. The crystal orbital overlap population (COOP) curve for Cu−Cu bonds less than 2.60 Å shows that orbitals at the Fermi level have significant Cu−Cu bonding overlap (values between 0.04 and 0.06 for Cu−Cu overlap populations are obtained). The density of atoms in this structure, $(14.4\ Å^3)^{-1}$, gives rise to broad dispersion of the Cu and P bands, and there is no measurable energy gap in the total DOS.

Table 4. Atomic Orbital Parameters Used in Extended Hückel Calculations

atom	orbital	H_{ii} (eV)	ϵ_1	C_1	ϵ_2	C_2
Ba	6s	−7.67	2.14			
	6p	−5.01	2.08			
Cu	4s	−11.40	2.20			
	4p	−6.06	2.20			
	3d	−14.00	5.95	0.5933	2.30	0.5744
P	3s	−18.60	1.88			
	3p	−12.50	1.63			

We have also calculated the total DOS and COOP curves for $BaCu_8P_4$. Our calculations also suggest this compound to show metallic behavior, but note the energy gap that occurs just above the Fermi level. The valence band is nearly full (it is four electrons per formula unit short of being completely occupied). Unlike $BaCu_{10}P_4$, however, the maximum Cu−Cu overlap population is calculated to be 0.03, with most of the values near 0.015. The Cu−P COOP curve reveals that Cu−P bonding is optimized, as the Fermi level intersects the point at which the orbitals change from Cu−P bonding to Cu−P antibonding. This effect in the Cu−P COOP curve is similar to what is observed in so-called "metallic Zintl phases".[22,23]

Finally, we want to address the distribution of electron density in these two compounds. Traditional methods of electron counting would formulate $BaCu_{10}P_4$ as formally closed-shell $Ba^{2+}(Cu^+)_{10}(P^{3-})_4$, whereas $BaCu_8P_4$ may be expressed as $Ba^{2+}(Cu_8)^{10+}(P^{3-})_4$, which suggests a mixed-valent or intermediate valent situation for the second compound. Mulliken population analyses indicate that orbitals near the Fermi level involve significant mixtures of Cu 3d, 4s and P 3p atomic orbitals. Furthermore, all Cu atoms in both structures obtain similar populations (10.97 in $BaCu_{10}P_4$ and 10.92 in $BaCu_8P_4$).

Therefore, we conclude that both $BaCu_{10}P_4$ and $BaCu_8P_4$ show metallic character but for different reasons from their corresponding electronic structures. In $BaCu_{10}P_4$, the density of Cu atoms led to broad dispersion of the conduction band and no discernible energy gap in the DOS, although the formal electron count gives a closed-shell configuration for all atoms. In $BaCu_8P_4$, metallic character is expected because the valence band is incompletely occupied. The structure leads to optimized Cu−P bond strengths.

Acknowledgment. This research was supported by the National Science Foundation (DMR-9201041). J.C. was a participant in the Summer Program in Solid State Chemistry for Undergraduates and Faculty (NSF-DMR9300695).

Supporting Information Available: Listing of complete crystal data, anisotropic displacement coefficients, and calculated versus experimental powder diffraction data (5 pages). Ordering information is given on any current masthead page.

IC961347Z

(22) Corbett, J. D. In *Chemistry, Structure and Bonding of Zintl Phases and Ions*; Kauzlarich, S. M., Ed.; VCH: New York, 1996.
(23) Miller, G. J. In *Chemistry, Structure, and Bonding of Zintl Phases and Ions*; Kauzlarich, S. M., Ed.; VCH: New York, 1996.